Available online at www.sciencedirect.com
ScienceDirect
Journal of Hazardous Materials 155 (2008) 206–215
Journal of Hazardous Materials
www.elsevier.com/locate/jhazmat

Defluoridation chemistry of synthetic hydroxyapatite at nano scale: Equilibrium and kinetic studies

C. Sairam Sundaram [a], Natrayasamy Viswanathan [b], S. Meenakshi [b,*]

[a] *Department of Science and Humanities, Karaikal, Polytechnic College, Karaikal 609609, Puducherry, India*
[b] *Department of Chemistry, Gandhigram Rural University, Gandhigram 624302, Tamilnadu, India*

Received 14 September 2007; received in revised form 15 November 2007; accepted 15 November 2007
Available online 22 November 2007

Abstract

This study describes the advantages of nano-hydroxyapatite (n-HAp), a cost effective sorbent for fluoride removal. n-HAp possesses a maximum defluoridation capacity [DC] of 1845 mg F^-/kg which is comparable with that of activated alumina, a defluoridation agent commonly used in the indigenous defluoridation technology. A new mechanism of fluoride removal by n-HAp was proposed in which it is established that this material removes fluoride by both ion-exchange and adsorption process. The n-HAp and fluoride-sorbed n-HAp were characterized using XRD, FTIR and TEM studies. The fluoride sorption was reasonably explained with Langmuir, Freundlich and Redlich–Peterson isotherms. Thermodynamic parameters such as ΔG°, ΔH°, ΔS° and E_a were calculated in order to understand the nature of sorption process. The sorption process was found to be controlled by pseudo-second-order and pore diffusion models. Field studies were carried out with the fluoride containing water sample collected from a nearby fluoride endemic area in order to test the suitability of n-HAp material as a defluoridating agent at field condition.

Keywords: Defluoridation; n-HAp; Langmuir; Freundlich; Redlich–Peterson; Pseudo-first-order; Pseudo-second-order; Particle and pore diffusion; Adsorption; Ion-exchange

1. Introduction

Fluoride ion in drinking water is known for both beneficial and detrimental effects on health. Consumption of drinking water containing excessive fluoride above 1.5 ppm leads to different forms of fluorosis. Removal of fluoride from water sources is of great scientific and practical interest. Fluoride from drinking water can be removed by either ion-exchange/adsorption process or by coagulation and precipitation process. Based on these processes several defluoridation methods have been proposed. These involve use of alum, lime, aluminium sulphate, magnesite, dolomite, activated alumina and synthetic tri-calcium phosphates etc. [1,2]. Recently membrane process such as reverse osmosis [3], electrodialysis [4], nanofiltration [5] and Donnan dialysis [6] were investigated to reduce concentration of fluoride in water.

Nanomaterials offer new possibilities to chemists. All aspects determining chemistry are modified in the nano scale. The surface properties, electronic structure, coordination etc., get modified when material dimensions reach the nanoscale. Traditional chemistry of the materials may completely become newer and novel chemistry may evolve as a function of size. Nanoparticles could be effectively employed for the removal of toxic chemicals from water as most of the toxic chemicals are removed by adsorption which depends on the surface site. n-HAp is widely used in the process of water treatment. Research works on the removal of cadmium, oxovanadium, cobalt, lead and zinc using hydroxyapatite (HAp) have been reported [7–11]. The authors in a recent paper reported that the adsorption mechanism is the more favorable mechanism for fluoride removal [12]. Hence in the present study, an attempt has been made to study the defluoridation efficiency of synthesized hydroxyapatite (HAp) at nano scale. Though the removal of fluoride using HAp [13,14] has been reported earlier, the authors felt that the use of n-HAp could definitely give a new dimension in the field of defluoridation, hence defluoridation experiments were carried out using the synthesized n-HAp.

HAp is a calcium phosphate based bioceramic and used in the medical field as it is the main component of the hard tissues of living bodies such as bones, teeth, etc. [15]. n-HAp is synthesized

* Corresponding author. Tel.: +91 451 2452371; fax: +91 451 2454466.
E-mail address: drs_meena@rediffmail.com (S. Meenakshi).

0304-3894/$ – see front matter © 2007 Elsevier B.V. All rights reserved.
doi:10.1016/j.jhazmat.2007.11.048

by a variety of ceramic processing routes including precipitation, sol–gel, hydrothermal processing routes, etc. [16]. However, the precipitation method appears more favourable, since the method of preparation is very simple, cost effective and eco-friendly which in turn make the process easily acceptable by the users.

In the present study, n-HAp was synthesized in the laboratory by precipitation method and defluoridation studies were carried out under various equilibrating conditions like the effect of contact time, dose, pH and in presence of competitor anions. The equilibrium and kinetic studies of defluoridation of n-HAp were thoroughly discussed which would definitely throw more light in understanding the defluoridation mechanism of n-HAp.

2. Materials and methods

2.1. Synthesis of n-HAp

Synthesis of n-HAp involves the reaction of calcium hydroxide and orthophosphoric acid with a Ca/P ratio close to 1.67. pH level of the reaction should be maintained at 7.5 otherwise it may lead to the formation of calcium monophosphate and calcium dehydrates [17]. The synthesis involved the initial formation of 0.5 M calcium hydroxide suspension. The suspension was vigorously stirred degassed and heated for 1 h before and during the acid addition. Then 0.3 M orthophosphoric acid was added dropwise at a drip rate of 1–2 drops to form a gelatinous precipitate at 40–42 °C. The pH level was controlled by the addition of NH_4OH solution. The precipitate was left in the mother solution overnight and supernant was decanted. The precipitate was washed with distilled water and then oven dried at 80 °C overnight. Then it was calcined at 400 °C to get a fine n-HAp ($Ca_{10}PO_4(OH)_2$) powder.

2.2. Characterisation of n-HAp

The synthesized n-HAp powder was characterized by transmission electron microscope (TEM), X-ray diffraction (XRD) and fourier transform infrared spectrometer (FTIR). The size and shape of n-HAp was measured by TEM (CM 200-PANalytical make). XRD spectra of synthesized n-HAp were identified by X'per PRO model-PANalytical make. XRD was used to determine the crystalline phases present in n-HAp. FTIR spectra of the samples as solid by diluting in KBr pellets were recorded with JASCO-460 plus model. The results of FTIR spectrometer were used to confirm the functional groups present and also fluoride sorption on the n-HAp.

2.3. Adsorption experiments

The sorption isotherm and kinetic experiments were performed by batch equilibration method. Stock solution of sodium fluoride containing 100 mg/L was prepared and this was used for fluoride sorption experiments. The batch adsorption experiments were carried out by mixing 0.25 g of n-HAp with 50 mL of 10 mg/L as initial fluoride concentration. The contents were shaken thoroughly using a thermostated shaker rotating at a speed of 200 rpm. The solution was then filtered and the residual fluoride ion concentration was measured using expandable ion analyser EA 940 and the fluoride ion selective electrode BN 9609 (USA make). The pH measurements were carried out with the same instrument with pH electrode. The kinetic and thermodynamic parameters of the adsorption were established by conducting the experiments at 303, 313 and 323 K in a temperature controlled mechanical shaker. The defluoridation capacity [DC] of the sorbents were studied at different conditions like various mass of sorbents, contact time of the sorbent for maximum defluoridation, pH of the medium and the effect of co-anions on defluoridation. The concentrations of NO_3^- and SO_4^{2-} ions were determined using UV–vis spectrophotometer (PerkinElmer – Lambda 35) [18]. All other water quality parameters were analysed by using standard methods [18]. The pH at zero point charge (pH_{zpc}) of n-HAp was measured using the pH drift method [19].

Computations were made using Microcal Origin (Version 6.0) software. The goodness of fit was discussed using regression correlation coefficient (r) and coefficient of determination (r^2).

3. Results and discussion

3.1. Characterisation of the sorbent

In order to characterize n-HAp, XRD, FTIR and TEM analysis were carried out on synthesized n-HAp and fluoride treated samples. The XRD pattern of synthesized n-HAp and the sample treated with fluoride was presented in Fig. 1a and b, respectively.

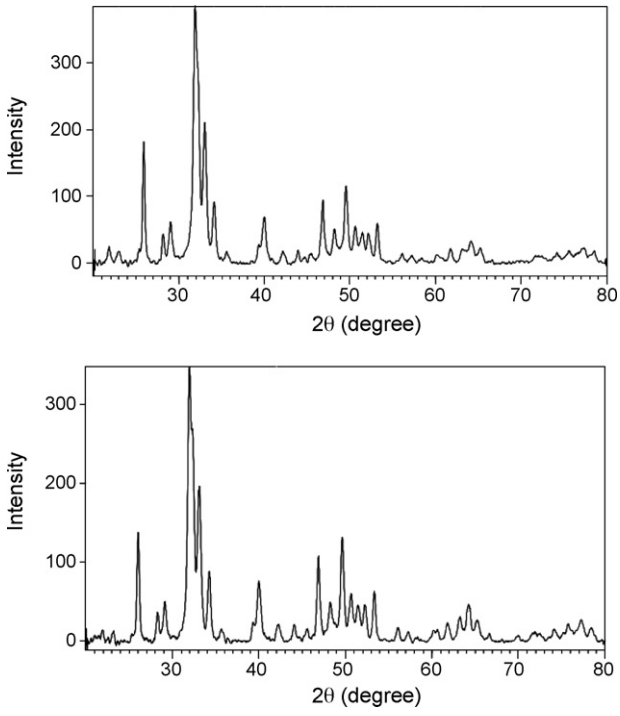

Fig. 1. XRD patterns of (a) n-HAp and (b) fluoride sorbed n-HAp.

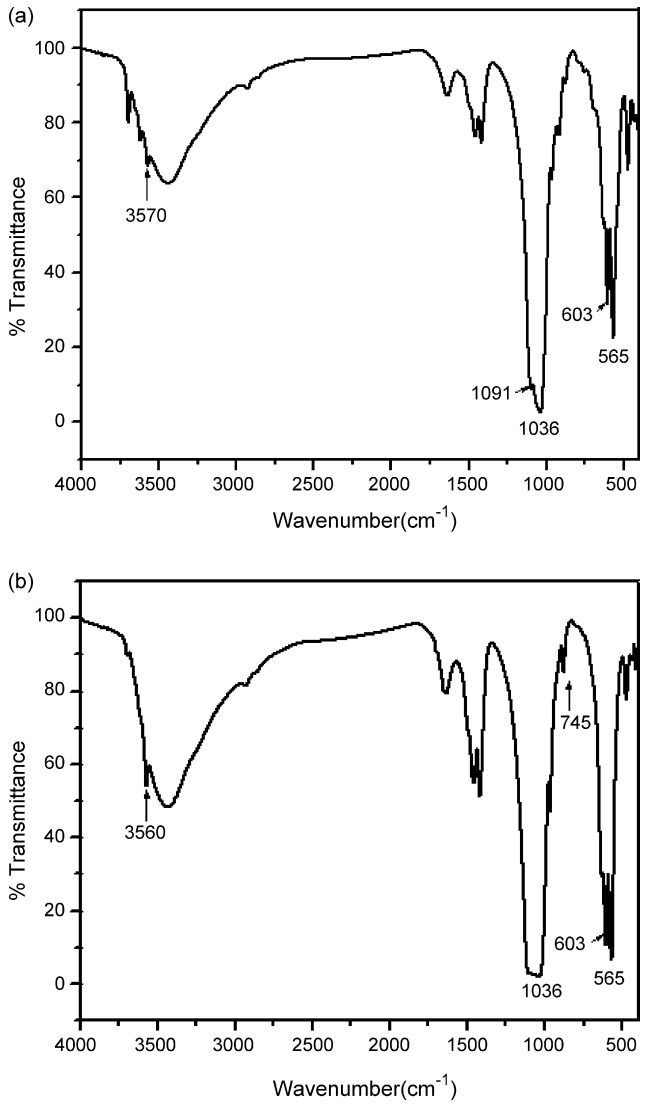

Fig. 2. FTIR spectra of (a) n-HAp and (b) fluoride treated n-HAp.

The crystalline peaks at $2\theta = 25.9°, 32°, 33°, 35.5°$ and 40° confirm the formation of hydroxyapatite structure [20]. There is no marked change in the XRD pattern of n-HAp after treatment with fluoride. Similar results are reported by Diaz-Nava et al. [21] while studying the fluoride sorption on zeolites.

Fig. 2a and b represents FTIR spectra of the samples before and after treatment with fluoride. The bands at 3570 cm^{-1} belong to the stretching vibrations of hydroxyl. The bands of 1040, 603 and 566 cm^{-1} belong to the phosphate stretching and bending vibrations, respectively [22]. There is a reduction in the intensity of –OH bands at 3570 and 630 cm^{-1} with some displacement to lower frequencies in fluoride treated n-HAp which may be due to fluoride adsorption/exchange. The apparition of new band at 745 cm^{-1} in fluoride treated n-HAp confirms the formation of O–H···F bond.

TEM micrographs of n-HAp powder were presented in Fig. 3a–c respectively. The size of the powder is about 200 nm with cylindrical rod like shape. The particles are of homogeneous microstructure and formed a uniform nanomaterial.

3.2. Effect of contact time and dose

The sorption of fluoride ion on n-HAp has been investigated as a function of contact time in the range of 10–60 min with 10 mg/L as initial fluoride concentration at room temperature. The effect of defluoriation capacity (DC) with contact time is shown in Fig. 4. It is evident that almost saturation was reached after 30 min. Hence 30 min was fixed as the period of contact for further studies. If the sorption process is only controlled by ion exchange mechanism, the saturation of the material would have been reached very soon. But n-HAp reached saturation only after 30 min suggesting that the process is also governed by adsorption which is rather slow than the ion-exchange process [12,23]. In order to fix the optimum dosage defluoridation experiments were carried out with various dosages of n-HAp ranging from 0.1 to 1.0 g with 10 mg/L as initial fluoride concentration and the results were given in Fig. 5. As it is obvious, the percent fluoride removal increases with increase in the dose of the sorbent due to more active sites with an increase in amount of sorbent [24]. The optimum dosage was fixed as 0.25 g for further studies as this dosage found to bring down the level of fluoride within the tolerance limit.

3.3. Effect of pH

The pH of the aqueous solution plays an important role which controls the adsorption at the water adsorbent interface [25]. Therefore the adsorption of fluoride on the n-HAp was examined at various pH ranges ranging from 3 to 11 with 10 mg/L as initial fluoride concentration at room temperature and was presented in Fig. 6. The pH of the working solution is controlled by adding sufficient HCl/NaOH solution. It can be inferred that fluoride removal decreases with increasing pH where the maximum DC is recorded as 1845 mgF^-/kg at pH 3 and only 570 mgF^-/kg was removed at pH 11. Similar observations are observed by Karthikeyan et al. [26] when activated alumina was used as sorbent. This can be explained due to the change in surface charge of the adsorbent. It is well established that the surface is highly protonated in acidic medium and therefore maximum fluoride removal in acidic medium is attributed to the gradual increase in attractive forces between positively charged surface and negatively charged fluoride ions. Lower DC in alkaline medium can be explained by the fact that the surface acquires negative charge in alkaline pH and hence there is a repulsion between the negatively charged surface and fluoride. This argument is very well supported by zero point charge studies (cf. Fig. 7). The pH_{zpc} value of n-HAp was found to be 7.88. Chemisorption occurs below the pH_{zpc} value and above pH_{zpc} value it will be physisorption in addition to ion exchange. This mechanism of fluoride removal is explained in Schemes 1–3.

3.4. Effect of other anions

The DC of n-HAp in presence of competing anions like sulphate, chloride, nitrate and bicarbonate which are usually present in water was experimentally verified with the concen-

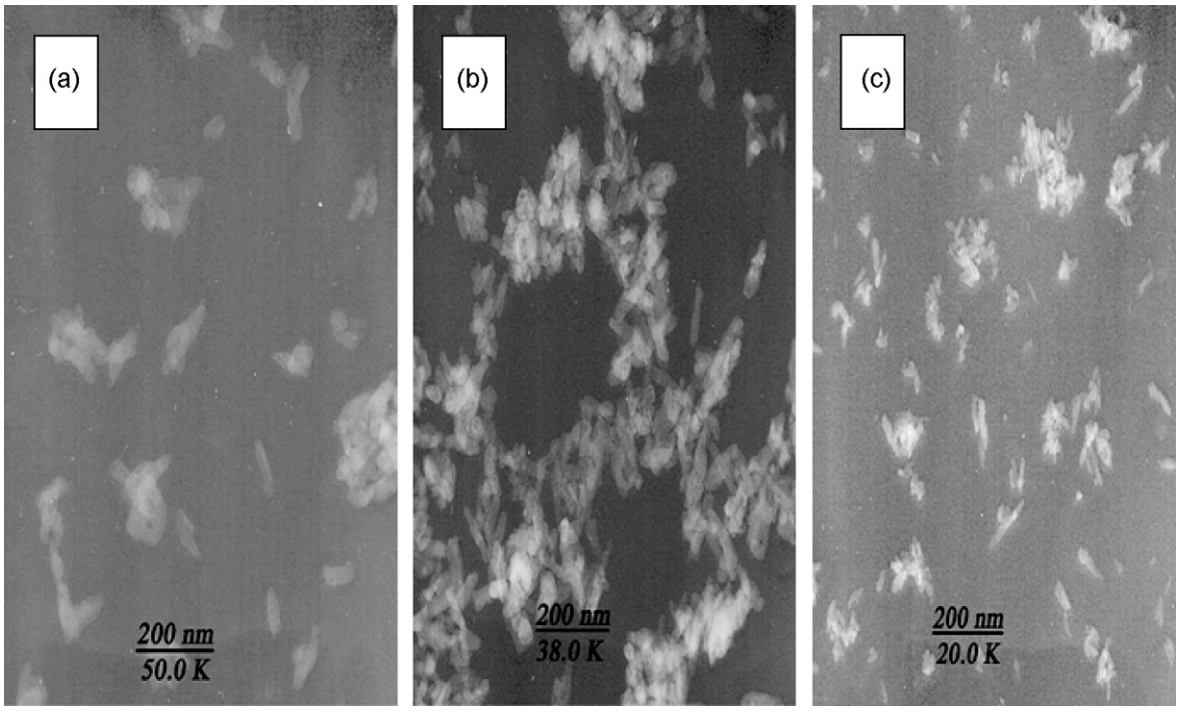

Fig. 3. (a–c) TEM images of n-HAp.

trations of anions ranging from 100 to 500 mg/L with 10 mg/L as initial fluoride concentration at 303 K. Fig. 8 shows the effect of common anions on DC of n-HAp. It can be inferred that there is no significant influence on DC of the material in the presence of Cl^-, SO_4^{2-} and NO_3^- ions. However, in presence of bicarbonate ion the DC decreased from 1290 to 856 mgF^-/kg. Hence from the above discussions it can be concluded that the bicarbonate ions will compete with fluoride ions during sorption. A similar interfering role on DC by the bicarbonate ion was reported in the case of defluoridation property of activated alumina and montmorillonite clay [26,27].

3.5. Adsorption isotherms

The sorption isotherms express the specific relation between the concentration of sorbate and its degree of accumulation onto sorbent surface at constant temperature. The fluoride sorption capacity of n-HAp has been evaluated using three different isotherms namely Langmuir, Freundlich and Redlich–Peterson isotherms.

The linear form of Freundlich isotherm [28] is represented in Table 1. q_e is the amount of fluoride adsorbed per unit weight of the sorbent at equilibrium (mg/g), C_e is the equilibrium concentration of fluoride in solution (mg/L), k_F is a measure of

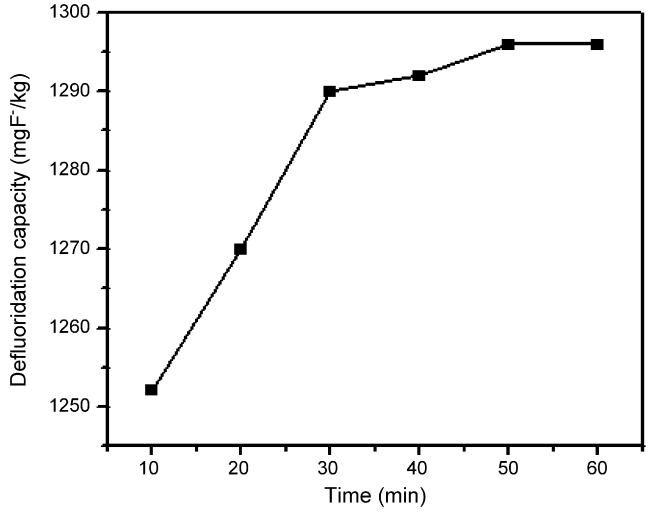

Fig. 4. Effect of contact time on the DC of n-HAp.

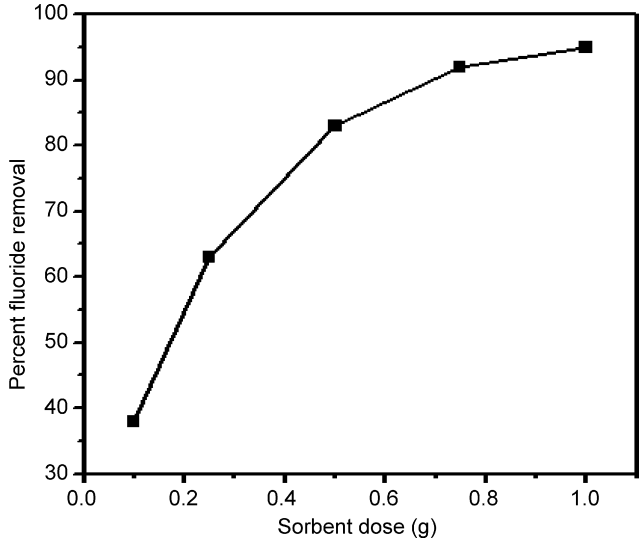

Fig. 5. Effect of sorbent dose in the percent fluoride removal of n-HAp.

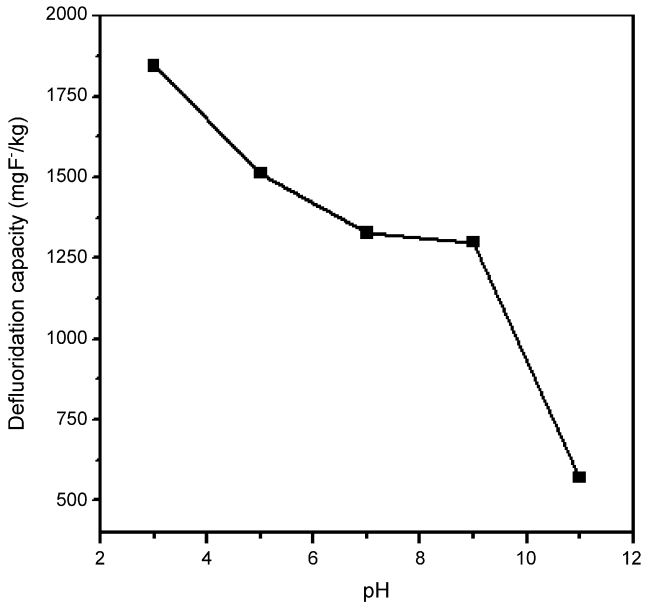

Fig. 6. Effect of pH.

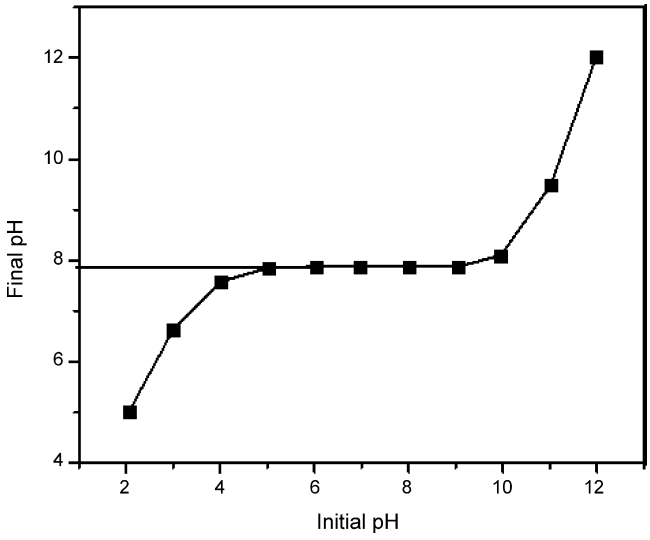

Fig. 7. Determination of pH_{zpc} of n-HAp.

$$\underset{\text{n-HAp}}{Ca_{10}(PO_4)_6(OH)_2} + n\,F^- \Longrightarrow \underset{\text{Hydrogen bonding}}{Ca_{10}(PO_4)_6(OH)_2\text{---}F_n^-}$$

Scheme 1. Fluoride removal of n-HAp by adsorption mechanism.

$$\underset{\text{n-HAp}}{Ca_{10}(PO_4)_6(OH)_2} + n\,F^- \xRightarrow[\text{Medium}]{\text{Acidic}} \underset{\text{Hydrogen bonding}}{Ca_{10}(PO_4)_6(OH^+)_2\text{---}F_n^-}$$

Scheme 2. Mechanism of fluoride removal in acidic medium.

$$\underset{\text{n-HAp}}{Ca_{10}(PO_4)_6(OH)_2} + 2\,F^- \Longrightarrow \underset{\text{Fluoroapatite}}{Ca_{10}(PO_4)_6F_2} + 2\,OH^-$$

$$\underset{\text{n-HAp}}{Ca_{10}(PO_4)_6(OH)_2} + F^- \Longrightarrow \underset{\text{Hydroxyfluoroapatite}}{Ca_{10}(PO_4)_6FOH} + OH^-$$

Scheme 3. Fluoride removal of n-HAp by ion-exchange mechanism.

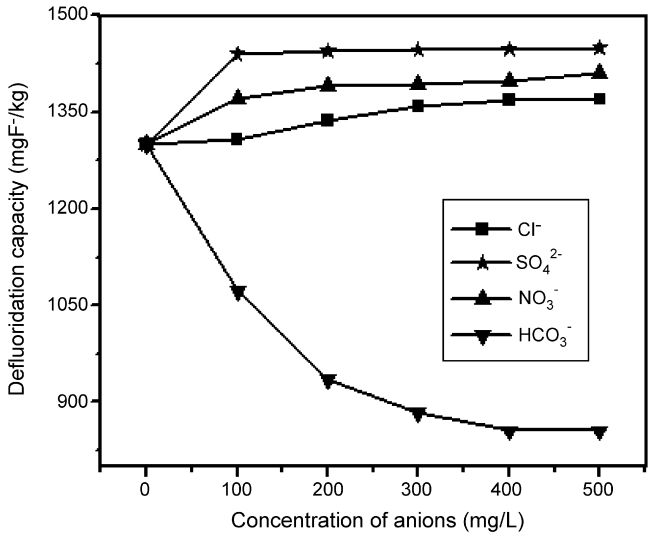

Fig. 8. Effect of competitor anions in the DC of n-HAp.

adsorption capacity and $1/n$ is the adsorption intensity. The Freundlich isotherm constants k_F and n were calculated from the slope and intercept of the plot of $\log q_e$ versus $\log C_e$ and were presented in Table 2. The values of $1/n$ are lying between 0.1 and 1.0 and the n value lying in the range of 1–10 confirms the favourable conditions for adsorption [12].

Langmuir isotherm [29] model has four types and are listed in Table 1. The sorption capacity (Q°) is the amount of adsorbate at complete monolayer coverage (mg/g), it gives the maximum sorption capacity of sorbent and b (L/mg) is the Langmuir isotherm constant that relates to the energy of adsorption. The respective values of Q° and b were determined from the slope and intercept of the straight line plot of C_e/q_e versus C_e and are presented in Table 2. From Table 2 it is clear that the higher r values for the sorption of fluoride on n-HAp were shown by Type I and Type II Langmuir isotherms.

In order to find out the feasibility of the isotherm, the essential characteristics of the Langmuir isotherm can be expressed in terms of a dimensionless constant separation factor or equilibrium parameter, R_L [30],

$$R_L = \frac{1}{1 + bC_o}, \tag{1}$$

where b is the Langmuir isotherm constant and C_o is the initial concentration of fluoride (mg/L). The R_L (Eq. [1]) values lying between 0 and 1 calculated from Langmuir models are shown in Table 2 indicates the favorable conditions for adsorption.

Redlich–Peterson isotherm [31] is a three parameter isotherm which incorporates the features of both Langmuir and Freundlich isotherms and its linear form is shown in Table 1. The isotherm constants A, B and g can be evaluated from the linear form of the Redlich–Peterson equation using a trial-and-error optimization method and were presented in Table 2. A general trial-and-error procedure which is applicable to computer operation was developed to determine the regression coefficient (r) for a series of values of A for the linear regression of $\ln C_e$ on $\ln [A(C_e/q_e) - 1]$ and to obtain the best value of A which yields a maximum optimized value of r and the respective values of g

Table 1
Isotherms with linear forms and their plots

Isotherms		Linear form	Plot
Freundlich	$q_e = k_F C_e^{1/n}$	$\log q_e = \log k_F + \frac{1}{n} \log C_e$	$\log q_e$ vs. $\log C_e$
Langmuir-1	$q_e = \frac{Q^\circ b C_e}{1 + bC_e}$	$\frac{C_e}{q_e} = \frac{1}{Q^\circ b} + \frac{C_e}{Q^\circ}$	$\frac{C_e}{q_e}$ vs. C_e
Langmuir-2		$\frac{1}{q_e} = \left[\frac{1}{Q^\circ b}\right] \frac{1}{C_e} + \frac{1}{Q^\circ}$	$\frac{1}{q_e}$ vs. $\frac{1}{C_e}$
Langmuir-3		$q_e = Q^\circ - \left[\frac{1}{b}\right] \frac{q_e}{C_e}$	q_e vs. $\frac{q_e}{C_e}$
Langmuir-4		$\frac{q_e}{C_e} = bQ^\circ - bq_e$	$\frac{q_e}{C_e}$ vs. q_e
Redlich–Peterson	$q_e = \frac{AC_e}{1 + BC_e^g}$	$\ln\left(A\frac{C_e}{q_e} - 1\right) = g \ln C_e + \ln B$	$\ln\left(A\frac{C_e}{q_e} - 1\right)$ vs. $\ln C_e$

and B were determined from the slope and intercept of the plot $\ln C_e$ versus $\ln [A(C_e/q_e)-1]$. It can be seen that the values of g are close to unity which suggests the isotherms are approaching Langmuir model [32].

3.6. Chi-square analysis

To identify the suitable isotherm model for the sorption of fluoride on the n-HAp, this analysis has been carried out. The chi-square statistic test is basically the sum of the squares of the differences between the experimental data and data obtained by calculating from models, with each squared difference divided by the corresponding data obtained by calculating from the models. The equivalent mathematical statement is:

$$\chi^2 = \sum \frac{(q_e - q_{e,m})^2}{q_{e,m}}, \quad (2)$$

where $q_{e,m}$ is equilibrium capacity obtained by calculating from the model (mg/g) and q_e is experimental data of the equilibrium capacity (mg/g). If the data from the model are similar to the experimental data, χ^2 will be a small number, while if they differ; χ^2 will be a bigger number. Therefore, it is necessary to also analyse the data set using the non-linear chi-square test to confirm the best-fit isotherm for the sorption system [12].

The corresponding chi-square values (Eq. (2)) for all the isotherms were presented in Table 2. From the chi-square values the best fit for the sorption of fluoride on n-HAp is in the following order:

$$\text{Langmuir}-1 > \text{Freundlich} > \text{Langmuir}-4 > \text{Langmuir}-3 > \text{Langmuir}-2 > \text{Redlich}-\text{Peterson}$$
$$\xrightarrow[\chi^2 \text{ values increases}]{}$$

The isotherm values fits well for both Langmuir-1 and Freundlich isotherms, but better fits to Langmuir-1 isotherm model indicating monolayer chemisorption being dominant.

Table 2
Isotherm parameters of n-HAp obtained at different temperatures

Isotherms	Parameters	303 K	313 K	323 K
Freundlich	$1/n$	0.318	0.215	0.285
	n	3.14	4.65	3.51
	$kF_{(mg/g)(L/mg)^{1/n}}$	0.554	0.706	0.687
	r	0.897	0.867	0.991
	χ^2	2.78E−3	2.18E−3	2.22E−4
Langmuir-1	Q° (mg/g)	1.288	1.204	1.457
	b (L/g)	0.533	1.026	0.612
	r	0.984	0.994	1.00
	R_L	0.211	0.122	0.189
	χ^2	1.94E−3	1.55E−3	1.12E−5
Langmuir-2	Q° (mg/g)	3.113	1.727	1.676
	b (L/g)	0.657	0.731	0.682
	r	0.945	0.926	1.00
	R_L	0.178	0.163	0.173
	χ^2	0.878	0.087	0.030
Langmuir-3	Q° (mg/g)	0.494	0.807	0.879
	b (L/g)	3.058	1.684	1.665
	r	0.835	0.846	0.999
	R_L	0.044	0.078	0.079
	χ^2	0.500	0.113	0.113
Langmuir-4	Q° (mg/g)	0.626	1.039	0.881
	b (L/g)	2.134	1.206	1.662
	r	0.835	0.846	0.999
	R_L	0.063	0.106	0.079
	χ^2	0.246	0.017	0.112
Redlich–Peterson	A (L/mg)	1.00	1.53	15.60
	g	0.90	1.12	1.15
	B (L/mg)^g	1.31	1.08	2.43
	r	0.932	0.986	0.841
	χ^2	0.489	0.668	0.507

3.7. Thermodynamic investigations

Thermodynamic parameters associated with the adsorption viz., standard free energy change (ΔG°), standard enthalpy change (ΔH°), standard entropy change (ΔS°) and activation energy (E_a) were calculated as follows.

The free energy of sorption process, considering the sorption distribution coefficient K_o, is given by the equation:

$$\Delta G^\circ = -RT \ln K_o, \quad (3)$$

where ΔG° is the standard free energy change (kJ/mol), T is the temperature in Kelvin and R is the universal gas constant (8.314 J mol^{-1} K^{-1}). The sorption distribution coefficient K_o for the sorption reaction was determined from the slope of the plot $\ln (q_e/C_e)$ against C_e at different temperatures and extrapolating

to zero C_e according to the method suggested by Khan and Singh [33].

The sorption distribution coefficient may be expressed in terms of ΔH° and ΔS° as a function of temperature:

$$\ln K_o = \frac{\Delta H^\circ}{RT} + \frac{\Delta S^\circ}{R}, \quad (4)$$

where ΔH° is the standard enthalpy change (kJ/mol) and ΔS° is standard entropy change (kJ/mol K). The values of ΔH° and ΔS° can be obtained from the slope and intercept of a plot of $\ln K_o$ against $1/T$.

A modified Arrhenius-type equation related to the surface coverage (θ) is sticking probability, S^*. This is a function of the adsorbate/adsorbent system, which is a measure of the potential of an adsorbate to remain on the adsorbent indefinitely [34] and it can be expressed as:

$$S^* = (1-\theta)\exp - \left(\frac{E_a}{RT}\right), \quad (5)$$

where θ is surface coverage,

$$\theta = \left(1 - \frac{C_e}{C_o}\right), \quad (6)$$

where C_o and C_e are the initial and equilibrium fluoride ion concentrations respectively. The plot of $\ln(1-\theta)$ against $1/T$ will give a linear plot with intercept of $\ln S^*$ and slope of E_a/R. The effect of temperature a major influencing factor in the sorption process, the sorption of n-HAp was monitored at three different temperatures 303, 313 and 323 K under the optimized condition and thermodynamic parameters viz., ΔG°, ΔH°, ΔS° and E_a were calculated from Eqs. (3)–(6) and presented in Table 3. It may be deduced from negative values of ΔG° indicates the sorption process is spontaneous. The positive value of ΔH° and E_a indicates the endothermic nature of the sorption process. The positive value ΔS° shows the increasing randomness during the sorption of fluoride ions onto n-HAp. The value of S^* is found to be 0.1 which is very close to zero indicates that the adsorption follows chemisorption [34].

3.8. Sorption dynamics

To understand the sorption mechanism such as mass transport and chemical reaction processes, two types of models viz., reaction-based and diffusion-based models were applied to test the fitness of experimental data [35]. The prediction of the batch sorption kinetics is necessary for the design of industrial adsorption column.

Table 3
Thermodynamic parameters obtained at different temperatures during fluoride sorption on n-HAp

Thermodynamic parameters		n-HAp
ΔG° (kJ mol^{-1})	303 K	−5.08
	313 K	−4.73
	323 K	−4.92
ΔH° (kJ mol^{-1})		7.63
ΔS° (kJ mol^{-1} K^{-1})		8.71
E_a (kJ mol^{-1})		4.58
S^*		0.10

Table 4
Lagergren constants for sorption of fluoride on n-HAp at different temperatures

C_o (mg/L)	Mass (g)	303 K		313 K		323 K	
		k_{ad} (min^{-1})	r	k_{ad} (min^{-1})	r	k_{ad} (min^{-1})	r
7	0.25	0.128	0.840	0.137	0.958	0.157	0.983
9	0.25	0.148	0.954	0.127	0.903	0.133	0.892
11	0.25	0.154	0.974	0.145	0.951	0.132	0.860
13	0.25	0.148	0.964	0.199	0.969	0.163	0.850

3.8.1. Reaction-based models

In order to investigate the sorption mechanism of fluoride removal, pseudo-first-order and pseudo-second-order kinetic models have been used at different experimental conditions.

A simple pseudo-first-order kinetic model [36] is represented as:

$$\log(q_e - q_t) = \log q_e - \frac{k_{ad}}{2.303}t, \quad (7)$$

where q_t is the amount of fluoride on the surface of the sorbent n-HAp at time t (mg/g) and k_{ad} is the equilibrium rate constant of pseudo-first-order sorption (min^{-1}). The straight-line plots of $\log(q_e - q_t)$ against t for different experimental conditions will give the value of the rate constants (k_{ad}). Linear plots of $\log(q_e - q_t)$ against t give straight line which indicates the applicability of Lagergren equation. The values of k_{ad} and the correlation coefficient (r) computed from these plots were given in Table 4. The pseudo-first-order model seems to be viable because of the higher correlation coefficient (r).

In addition, the pseudo-second-order model is also widely used. Though there are four types of linear pseudo-second-order kinetic models [37] the most popular linear form used has the equation:

$$\frac{t}{q_t} = \frac{1}{h} + \frac{t}{q_e}, \quad (8)$$

where $q_t = q_e^2 kt/(1 + q_e kt)$, amount of fluoride on the surface of the n-HAp at any time, t (mg/g), k is the pseudo-second-order rate constant (g/mg min), q_e is the amount fluoride ion sorbed at equilibrium (mg/g) and the initial sorption rate, $h = kq_e^2$ (mg/g min). The value of q_e (1/slope), k (slope^2/intercept) and h (1/intercept) of the pseudo-second-order equation can be found out experimentally by plotting t/q_t against t.

The fitness of the pseudo-second-order model (Eq. (8)) on the fluoride sorption on n-HAp was also analysed. The plot of t versus t/q_t gives a straight line with higher correlation coefficient r values, which is higher than that observed with pseudo-first-order model indicating the applicability of the pseudo-second-order model and the values are shown in Table 5. The values of q_e increased with increase in initial concentration and it also increased with increase in temperature. The values of rate constant (k) have also increased with temperature indicating chemisorption.

In a linear analysis, different linear forms of the same model would significantly affect calculations of the parameters [38]. According to Ho [37], a non-linear method could be a better way to obtain the kinetic parameters and would be able to avoid such errors. For the non-linear method, a trial and error procedure which is applicable to computer operation was developed to determine the pseudo-second-order rate parameters by optimization routine to maximize the coefficient of determination (r^2) between experimental data and pseudo-second-order model using the solver add-in with Microsoft's spreadsheet, Microsoft Excel.

In this study, the coefficient of determination, r^2 was calculated using Eq. (9) to test the best-fit of the linear and non-linear pseudo-second-order kinetic model to the experimental data:

$$r^2 = \sum \frac{(q_m - \bar{q}_t)^2}{(q_m - \bar{q}_t)^2 + (q_m - q_t)^2}, \quad (9)$$

where q_m is the amount of fluoride ion on the surface of the n-HAp at any time, t (mg/g) obtained from the second-order kinetic model, q_t is the amount of fluoride ion on the surface of the n-HAp at any time, t (mg/g) obtained from experiment and $\bar{q}_t$ is the average of q_t (mg/g). The coefficient of determination r^2 calculated from both linear and non-linear methods were presented in Table 5 with the experimental data for q_e, k and h. Higher values of r^2 in non-linear method indicates the better applicability of non-linear pseudo-second-order method than the linear one.

3.8.2. Diffusion-based models

For a solid–liquid sorption process, the solute transfer is usually characterised either by particle diffusion or pore diffusion control.

A simple equation for the particle diffusion controlled sorption process [12,39] is as follows:

$$\ln\left(1 - \frac{C_t}{C_e}\right) = -k_p t, \quad (10)$$

where k_p is the particle rate constant (min^{-1}). The value of particle rate constant is obtained by the slope of $\ln(1 - C_t/C_e)$ against t.

The pore diffusion model used here refers to the theory proposed by Weber and Morris [40,41]. The intraparticle diffusion equation is given below:

$$q_t = k_i t^{1/2}, \quad (11)$$

where k_i is the intraparticle rate constant (mg/g $min^{0.5}$). The slope of the plot of q_t against $t^{1/2}$ will give the value of intraparticle rate constant. On plotting q_t versus $t^{0.5}$ gives an initial curve followed by a straight line which indicates that two types of mechanisms are involved in the adsorption process. The initial curve represents the boundary layer effect while the linear part corresponds to intraparticle diffusion.

Both particle (Eq. (10)) and pore (Eq. (11)) diffusion models have been applied and the values of k_p and k_i were presented in Table 6. Higher r values in both the cases indicate the possibility of sorption process being controlled by both the particle and pore diffusion models.

3.9. Fitness of the sorption kinetic models

The assessment of the employed kinetic models for fitting the sorption data was made by calculating the squared sum of errors [SSE]. Lower values of SSE show better fit to sorption data and can give an indication of the sorption mechanism [12].

$$SSE = \sum \frac{(q_{t,e} - q_{t,m})^2}{q_{t,e}^2}, \quad (12)$$

where $q_{t,e}$ and $q_{t,m}$ are the experimental sorption capacity of fluoride (mg/g) at time t and the corresponding value which is obtained from the kinetic models. SSE values (Eq. (12)) of the reaction-based and diffusion-based kinetic models were computed and summarized in Table 7. It is assumed that the model which gives the lowest SSE values is the best model for this system and then the mechanism of sorption can be explained based on that model. It was observed from Table 7 that pseudo-second-order model and pore diffusion model seems to be better fit than the other two models (pseudo-first-order and particle diffusion models) for representing the kinetics of fluoride sorption on n-HAp.

3.10. Mechanism of fluoride sorption on n-HAp

The fluoride removal by n-HAp appears to be controlled by both adsorption and ion-exchange mechanisms. In fluoride solu-

Table 5
Comparison of the linear and non-linear methods of pseudo-second-order kinetic parameters of n-HAp based on coefficient of determination (r^2)

Methods	Parameters	303 K				313 K				323 K			
		7 mg/L	9 mg/L	11 mg/L	13 mg/L	7 mg/L	9 mg/L	11 mg/L	13 mg/L	7 mg/L	9 mg/L	11 mg/L	13 mg/L
Linear	q_e (mg/g)	0.804	0.961	1.098	1.068	0.881	1.034	1.101	1.115	0.915	1.046	1.162	1.252
	k (g/mg min)	0.412	0.670	0.452	0.479	0.613	0.652	0.735	0.460	1.034	1.125	0.441	0.315
	h (mg/g min)	0.266	0.618	0.545	0.546	0.475	0.698	0.891	0.572	0.865	1.230	0.596	0.494
	r	0.996	0.999	0.999	1.00	1.00	0.999	1.00	0.999	1.00	1.00	0.998	0.998
	r^2	0.838	0.783	0.745	0.761	0.782	0.848	0.799	0.724	0.774	0.872	0.846	0.786
Non-linear	q_e (mg/g)	0.729	0.891	0.989	0.961	0.802	0.983	1.046	0.975	0.869	1.009	1.087	1.127
	k (g/mg min)	0.406	0.664	0.445	0.473	0.959	0.649	0.731	0.452	1.030	1.123	0.438	0.311
	h (mg/g min)	0.216	0.527	0.435	0.436	0.617	0.627	0.800	0.430	0.777	1.144	0.517	0.394
	r^2	0.861	0.831	0.805	0.775	0.794	0.911	0.908	0.697	0.883	0.859	0.891	0.833

Table 6
Particle and pore diffusion model parameters for fluoride sorption at different initial concentrations with different temperatures

C_o (mg/L)	Mass (g)	303 K				313 K				323 K			
		Particle DM[a]		Pore DM[a]		Particle DM[a]		Pore DM[a]		Particle DM[a]		Pore DM[a]	
		k_p (min^{-1})	r	k_i (mg/g $min^{0.5}$)	r	k_p (min^{-1})	r	k_i (mg/g $min^{0.5}$)	r	k_p (min^{-1})	r	k_i (mg/g $min^{0.5}$)	r
7	0.25	0.012	0.979	0.058	0.981	0.012	0.984	0.049	0.995	0.010	0.932	0.036	0.958
9	0.25	0.009	0.956	0.048	0.972	0.010	0.989	0.043	0.993	0.007	0.970	0.030	0.984
11	0.25	0.001	0.961	0.064	0.972	0.008	0.941	0.046	0.961	0.010	0.985	0.057	0.974
13	0.25	0.007	0.975	0.063	0.991	0.008	0.959	0.066	0.978	0.011	0.975	0.085	0.985

[a] DM: diffusion model.

Table 7
The squared sum of errors (SSE) values of kinetic models employed for fluoride sorption on n-HAp

Kinetic models	303 K				313 K				323 K			
	7 mg/L	9 mg/L	11 mg/L	13 mg/L	7 mg/L	9 mg/L	11 mg/L	13 mg/L	7 mg/L	9 mg/L	11 mg/L	13 mg/L
Pseudo-first-order	2.7E−3	7.9E−3	4.8E−3	5.8E−3	8.9E−3	1.5E−3	1.1E−3	7.5E−5	9.4E−3	1.8E−2	8.5E−3	6.9E−4
Pseudo-second-order	2.7E−3	1.8E−3	3.6E−3	3.0E−3	2.9E−3	1.1E−3	1.3E−3	5.3E−3	1.2E−3	3.3E−3	1.8E−3	4.7E−3
Particle diffusion	0.707	0.750	0.968	0.795	0.697	0.732	0.770	0.769	0.730	0.797	0.733	0.710
Pore diffusion	0.416	0.600	0.532	0.528	0.554	0.662	0.665	0.527	0.686	0.769	0.599	0.455

tion, the F^- ions gets adsorbed onto the n-HAp surface as shown in Scheme 1.

In acidic medium, where the concentration of H^+ ion is high and therefore n-HAp surface acquires positive charge which in turn attracts more fluoride ions and hence there is a significant increase in DC at lower pH. This is illustrated in Scheme 2.

The nature of attractive force between n-HAp and fluoride ions as described above is confirmed by the FTIR results in which there is an emergence of new peak at 745 cm^{-1}, which is the characteristic of O–H···F vibration band in the fluoride sorbed n-HAp. As the pH increases surface slowly acquire negative charges which would repel fluoride ions and hence the fluoride removal by electrostatic attraction is ruled out in alkaline medium.

In addition, ion exchange mechanism is also involved in fluoride removal by n-HAp. The OH group present in the n-HAp is considered as the charge carrier and can get exchanged with F^- ions [42]. The mechanism of fluoride removal of n-HAp by ion exchange is represented in Scheme 3.

Hence it can be concluded that the fluoride removal by n-HAp is governed by both adsorption and ion-exchange mechanism and thus it can act as an effective defluoridating agent.

Table 8
Field trial results of n-HAp

Water quality parameters	Treatment	
	Before	After
F^- (mg/L)	2.33	0.47
pH	9.10	8.78
EC (ms/cm)	0.62	0.63
Cl^- (mg/L)	57.00	53.00
TH (mg/L)	70.00	0.00
TDS (mg/L)	465.00	453.00
Na (mg/L)	42.00	39.30
K (mg/L)	8.80	7.90

3.11. Field trial

The applicability of the n-HAp in the field condition was also tested with the sample taken from a nearby fluoride-endemic area. The results were presented in Table 8. The concentration of fluoride in the treated water is well within the tolerance limit and there is no significant change in other water quality parameters after treatment.

4. Conclusions

From the above discussions following conclusions were made, fluoride sorption on n-HAp is spontaneous and endothermic. The DC of n-HAp is significantly influenced by pH of the medium. There is no significant influence of other co-anions like chloride, nitrate and sulphate on the DC of n-HAp except bicarbonate ions. The mechanism of fluoride removal of n-HAp follows both adsorption and ion-exchange mechanism. The adsorption pattern follows both Langmuir and Freundlich isotherms, but better fits to Langmuir isotherm particularly Langmuir-1 model. The rate of reaction follows pseudo-second-order kinetics. A non-linear pseudo-second-order model would be a better way to obtain kinetic parameters. The sorption of fluoride ion on n-HAp occurs through intraparticle diffusion pattern. Field trials indicated that n-HAp can be effectively used as an efficient and cost effective defluoridating agent.

References

[1] P. Phantumvanit, Y. Songpaisan, I.J. Moller, A defluoridator for individual households, World Health Forum 9 (1988) 555–558.
[2] N.V. Rao, R. Mohan, C.S. Bhaskaran, Studies on defluoridation of water, J. Fluorine Chem. 41 (1998) 17–24.
[3] S.V. Joshi, S.H. Mehta, A.P. Rao, A.V. Rao, Estimation of sodium fluoride using HPLC in reverse osmosis experiments, Water Treat. 10 (1992) 307–312.

[4] S.K. Adihikary, U.K. Tipnis, W.P. Harkare, K.P. Govindan, Defluoridation during desalination of brackish water by electrodialysis, Desalination 71 (1989) 301–312.
[5] R. Simons, Trace element removal from ash dam waters by nanofiltration and diffusion dialysis, Desalination 89 (1993) 325–341.
[6] A. Dieye, Defluoridation des eaux par dialyse ionique croisee, Thesis, University Paris XII, 1995.
[7] G. Lusvardi, G. Malavasi, L. Menabue, M. Saladini, Removal of cadmium ion by means of synthetic hydroxyapatite, Waste Manage. 22 (2002) 853–857.
[8] E.D. Vega, J.C. Pedregosa, G.E. Narda, P.J. Morando, Removal of oxovanadium (IV) from aqueous solutions by using commercial crystalline calcium hydroxyapatite, Water Res. 37 (2003) 1776–1782.
[9] I. Smiciklas, S. Dimovic, I. Plecas, M. Mitric, Removal of Co^{2+} from aqueous solutions by hydroxyapatite, Water Res. 40 (2006) 2267–2274.
[10] B. Sandrine, N. Ange, B. Didier, C. Eric, S. Patrick, Removal of aqueous lead ions by hydroxyapatite: equilibria and kinetic process, J. Hazard. Mater. 139 (2007) 443–446.
[11] R.R. Sheha, Sorption behaviour of Zn(II) ions on synthesized hydroxyapatites, J. Colloid Interface Sci. 310 (2007) 18–26.
[12] S. Meenakshi, N. Viswanathan, Identification of selective ion exchange resin for fluoride sorption, J. Colloid Interface Sci. 308 (2007) 438–450.
[13] X. Fan, D.J. Parker, M.D. Smith, Adsorption kinetics of fluoride on low cost materials, Water Res. 37 (2003) 4929–4937.
[14] L.E.L. Hammari, A. Laghzizil, P. Barboux, K. Lahlil, A. Saoiabi, Retention of fluoride ions from aqueous solution using porous hydroxyapatite: structure and conduction properties, J. Hazard. Mater. 114 (2004) 41–44.
[15] L.L. Hench, Biomaterials a forecast for the future, Biomaterials 19 (1998) 1419–1423.
[16] P. Luo, Methods for synthesizing HA powders and bulk materials, US Patent 5858318, 1996.
[17] M.G.S. Murray, J. Wanj, C.B. Ponton, P.M. Marquis, An improvement in processing of hydroxyapatite ceramics, J. Mater. Sci. 30 (1995) 3061–3074.
[18] APHA, Standard Methods for the Examination of Water and Waste Water, American Public Health Association, Washington, DC, 2005.
[19] Y.F. Jia, B. Xiao, K.M. Thomas, Adsorption of metal ions on nitrogen surface functional groups in activated carbons, Langmuir 18 (2002) 470–478.
[20] W. Jie, L. Yubao, Tissue engineering scaffold material of nano-apatite crystals and polyamide composite, Eur. Poly. J. 40 (2004) 509–515.
[21] C. Diaz-Nava, M.T. Olguin, M. Solache-Rios, Water defluoridation by Mexican heulandite-clinoptilolite, Sep. Sci. Tech. 37 (2002) 3109–3128.
[22] F. Chen, Z. Wang, C. Lin, Preparation and characterization of nano-sized hydroxyapatite particles and hydroxyapatite/chitosan nano-composite for use in biomedical materials, Mater. Lett. 57 (2002) 858–861.
[23] K.S. Low, C.K. Lee, A.C. Leo, Removal of metals from electroplating wastes using banana pith, Bioresource Technol. 51 1995) 227–231.
[24] A. Boualia, A. Mellah, T. Aissaoui, K. Menacer, A. Silem, Adsorption of organic matter contained in industrial H_3PO_4 onto bentonite: batch-contact time and kinetic study, Appl. Clay Sci. 7 (1993) 431–445.
[25] S. Meenakshi, Anitha Pius, G. Karthikeyan, B.V. Appa Rao, The pH dependence of efficiency of activated alumina in defluoridation of water, Indian. J. Environ. Prot. 11 (1991) 511–513.
[26] G. Karthikeyan, A. Shummuga Sundarraj, S. Meenakshi, K.P. Elango, Adsorption dynamics and the effect of temperature of fluoride at alumina-solution interface, J. Indian. Chem. Soc. 81 (2004) 461–466.
[27] G. Karthikeyan, Anitha Pius, G. Alagumuthu, Fluoride adsorption studies on montmoillonite clay, Indian J. Chem. Tech. 12 (2005) 263–272.
[28] H.M.F. Freundlich, Uber die adsorption in lösungen, Z. Phys. Chem. 57A (1906) 385–470.
[29] I. Langmuir, The constitution and fundamental properties of solids and liquids, J. Am. Chem. Soc. 38 (1916) 2221–2295.
[30] T.W. Weber, R.K. Chakravorti, Pore and solid diffusion models for fixed bed adsorbers, J. Am. Inst. Chem. Eng. 20 (1974) 228–238.
[31] O. Redlich, D.L. Peterson, A useful adsorption isotherm, J. Phys. Chem. 63 (1959) 1024.
[32] Y.S. Ho, Isotherms for the sorption of lead onto peat: comparison of linear and non-linear methods, Polish J. Environ. Stud. 15 (2006) 81–86.
[33] A.A. Khan, R.P. Singh, Adsorption thermodynamics of carbofuran on Sn(IV) arsenosilicate in H^+, Na^+ and Ca^{2+} forms, Colloid and Surf. 24 (1987) 33–42.
[34] M. Horsfall, A.I. Spiff, Effects of temperature on the sorption of Pb^{2+} and Cd^{2+} from aqueous solution by caladium bicolour (Wild Cocoyam) biomass, Electron. J. Biotechnol. 8 (2005) 162–169.
[35] Y.S. Ho, J.C.Y. Ng, G. McKay, Kinetics of pollutant sorption by biosorbents: review, Sep. Purif. Methods 29 (2000) 189–232.
[36] S. Lagergren, Zur Theorie der sogenannten adsorption geloster stoffe, K. Sven. Vetenskapsakad. Handl. 24 (1898) 1–39.
[37] Y.S. Ho, Second-order-kinetic model for the sorption of cadmium onto tree fern: a comparison of linear and non-linear methods, Water Res. 40 (2006) 119–125.
[38] Y.S. Ho, Citation review of Lagergren kinetic rate equation on adsorption reactions, Scientometrics 59 (2004) 171–177.
[39] M. Chanda, K.F. O'Driscoll, G.L. Rempel, Sorption of phenolics onto cross-linked poly (4-vinylpyridine), React. Polym. 1 (1983) 281–293.
[40] W.J. Weber, J.C. Morris, Equilibria and capacities for adsorption on carbon, J. Sanitary Eng. Div. 90 (1964) 79–107.
[41] Y. Önal, C. Akmil-Başar, D. Eren, Ç. Sarıcı-Özdemir, T. Depci, Adsorption kinetics of malachite green onto activated carbon prepared from Tunçbilek lignite, J. Hazard Mater. 128 (2006) 150–157.
[42] H.G. McCann, Reactions of fluoride ion with hydroxyapatite, J. Biol. Chem. 201 (1952) 247–259.